

1997年12月31日

1997年12月31日

1997年12月31日

1997年12月31日

1997年12月31日

1997年12月31日

1997年12月31日

REPUBLIC OF ZIMBABWE
REPORT ON THE COOPERATIVE MINERAL
EXPLORATION OF SHAMVA AREA

PHASE II

JICA LIBRARY



1029804[01]

1481

MARCH 1985

JAPAN INTERNATIONAL COOPERATION AGENCY
METAL MINING AGENCY OF JAPAN

国際協力事業団	
受入 月日 '86. 2.26	534
登録No. 12481	66.1
	MPN

PREFACE

At the request of the Government of the Republic of Zimbabwe the Japanese Government planned a mineral exploration program consisting of several survey methods to examine the possibility of the existence of mineral deposits in the Shamva District located in the northeastern part of Zimbabwe; The Japanese Government entrusted the execution of the general plan to the Japan International Cooperation Agency (JICA), and in turn JICA entrusted the execution of this survey to the Metal Mining Agency of Japan (MMAJ) since this survey was a professional survey program of mineral exploration.

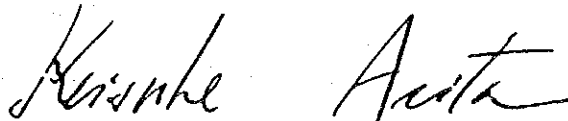
This year's program is the second year's one. MMAJ organized a survey team of three members and dispatched the team to Zimbabwe during the period from July 6 to November 19, 1984. The on-site survey was completed as scheduled with the cooperation of the Zimbabwe Government, particularly the Geological Survey Department of the Ministry of Mines.

This report describes the survey results of the second year program of the Shamva Project, and will form a part of a final report.

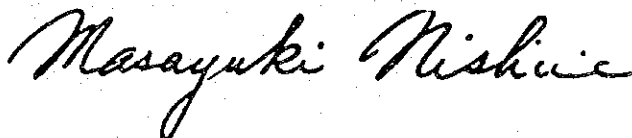
Lastly, we would like to express our heartfelt gratitude to the members concerned of the Zimbabwe Government, the Ministry of Foreign Affairs of Japan, the Ministry of International Trade and Industry of Japan, Japanese Embassy in Zimbabwe, and all of whom extended their kind cooperation to us in executing the above mentioned survey.

January, 1985

Keisuke Arita
President,
Japan International Cooperation Agency



Masayuki Nishiie
President,
Metal Mining Agency of Japan



ABSTRACT

ABSTRACT

The second year program was planned to examine the possible existence of mineralized zones at the subsurface in the areas, which were selected from the results of the first year program by applying modern geophysical survey methods, Controlled-Source Audio-Magnetotelluric (CSAMT) and Spectral Induced Polarization (SIP) Methods.

The survey program was conducted for 137 days from July 6 to November 19, 1984. The survey team consisted of three Japanese and two Zimbabweans.

The CSAMT survey covered the whole area. Areas C, D-1, D-2, and D-3, totalling 21km². Three hundred and six survey points were set up on a 300 meter grid pattern. Survey results showed strong low resistivity zones (below 10 ohm-meter) in several places. Judging from all geological, geochemical, and geophysical data, four SIP survey lines, A, B, C, D, of 10 km total line length with 300 survey points were chosen to examine the possibility of nickel sulphide mineralization associated with serpentines.

Several IP anomalies were detected as the result of the SIP survey. They were closely associated with low resistivity zones, serpentine host rocks, banded ironstones, and geochemical anomalies. It is therefore recommended to conduct a drilling program next year to examine some of the anomalous zones for the existence of nickel sulphide mineralized zones.

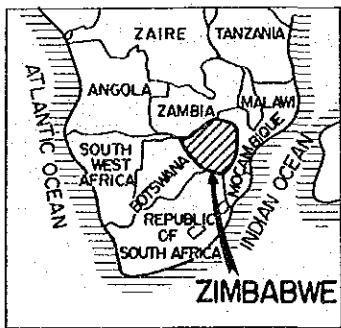
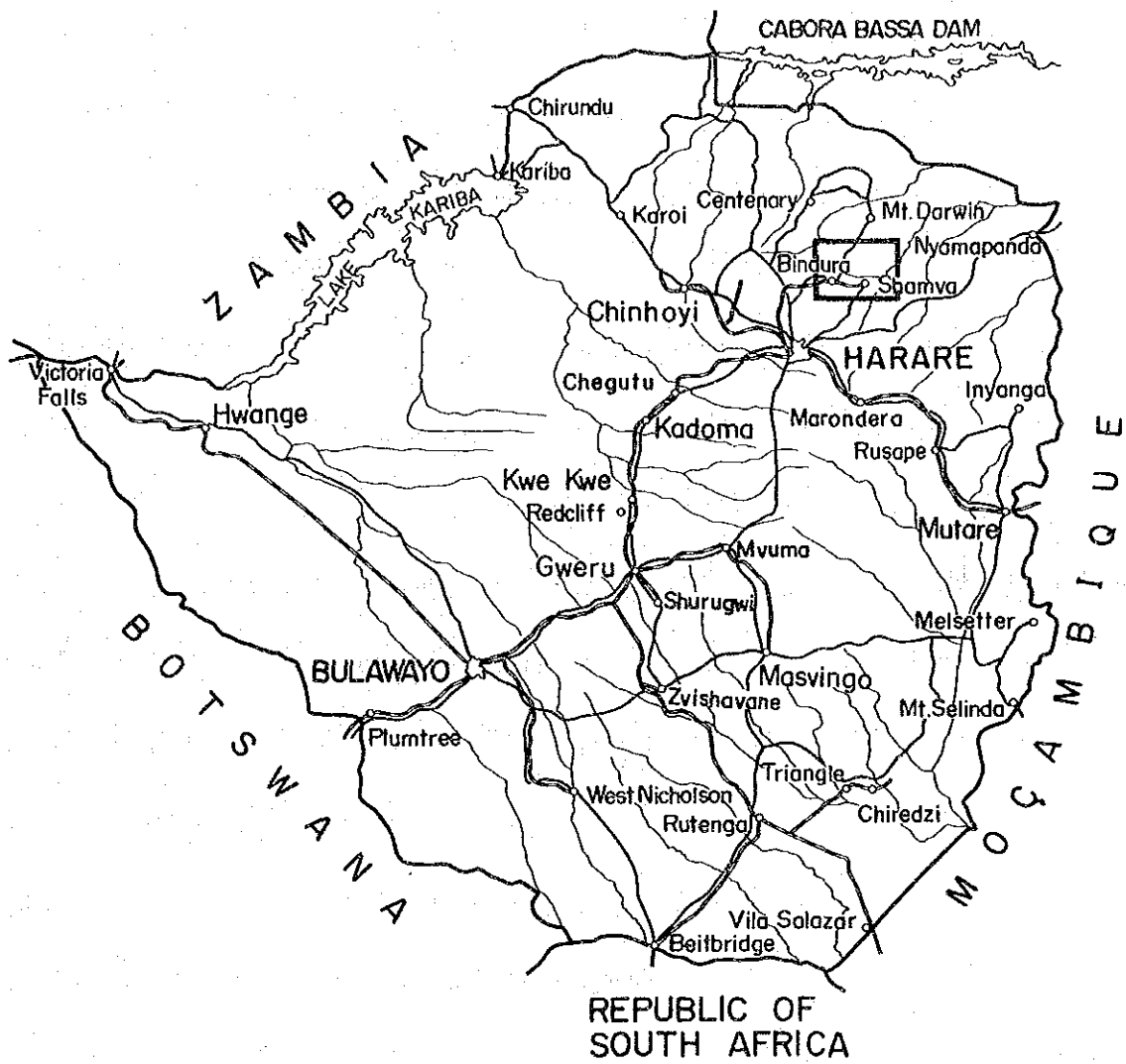
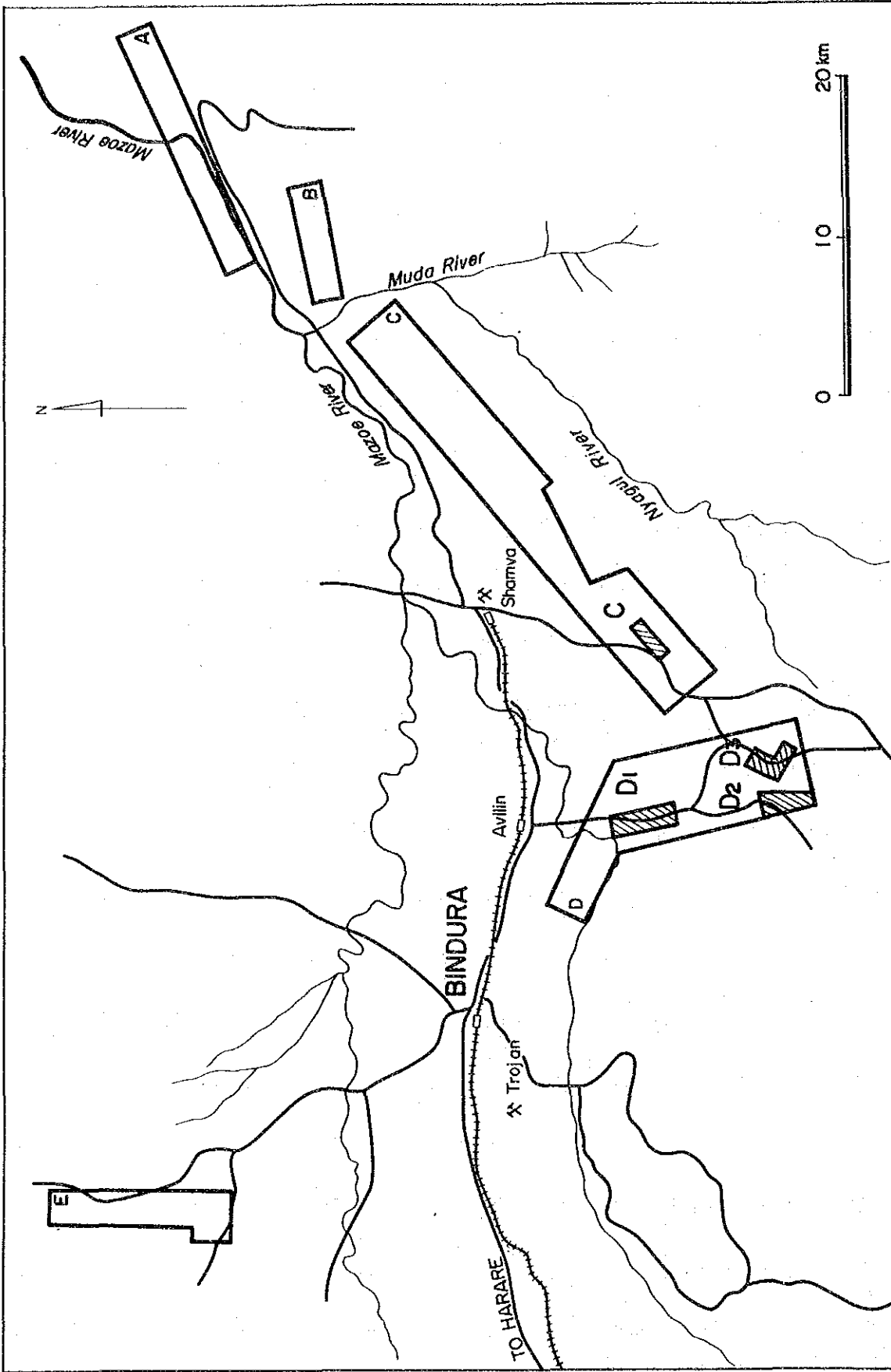


Fig. 1 Location Map of Project Area



Phase I (1983) Survey Area (Geological and Geochemical Surveys)

Phase II (1984) Survey Area (Geophysical Survey)

Fig. 2 Location Map of Survey Area (I)

CONTENT

	Page
PREFACE	
ABSTRACT	
LOCATION MAP	
PART 1. GENERAL DESCRIPTION	1
CHAPTER 1 INTRODUCTION	1
1-1 Purpose of the survey	1
1-2 Outline of the Survey	1
1-3 Organization of the Survey Team	2
CHAPTER 2 GENERAL CIRCUMSTANCES OF THE SURVEY AREA	3
2-1 Location and Transportation	3
2-2 Topography and Climate	3
2-3 General Social Circumstances	4
CHAPTER 3 GENERAL AND ECONOMIC GEOLOGY	5
3-1 General Geology	5
3-2 Economic Geology	6
PART 2. GEOPHYSICAL SURVEY	
CHAPTER 1 OUTLINE OF THE SURVEY	11
1-1 Survey Plan	11
1-2 Survey Method	11
1-3 Survey Record and Efficiency	12
CHAPTER 2 CSAMT SURVEY	13
2-1 Survey Method	13
2-1-1 Measuring Method	13
2-1-2 Instruments Used	15
2-1-3 Survey Point Positions	15

2-2	Data Processing and Analysis	16
2-2-1	Outline of CSAMT Method	16
2-2-2	Data Processing	18
2-2-3	Analytical Methods	20
2-3	Survey Result and Discussion	22
2-3-1	Survey Results	22
2-3-2	Discussion	27
CHAPTER 3	SIP SURVEY	29
3-1	Survey Method	29
3-1-1	Measuring Method	29
3-1-2	Instruments Used	30
3-1-3	Survey Line Setting	30
3-2	Data Processing and Analysis	31
3-2-1	Outline of SIP Method	31
3-2-2	Data Processing	33
3-2-3	Results of Measuring IP Properties	34
3-2-4	Analytical Method	34
3-3	Survey Result and Interpretation	37
3-3-1	Survey Results	37
3-3-2	Discussion	40
PART 3.	SYNTHETIC ANALYSIS	45
PART 4.	CONCLUSIONS AND RECOMMENDATION	49
CHAPTER 1	CONCLUSIONS	49
CHAPTER 2	RECOMMENDATION FOR THE THIRD YEAR PROGRAM	51
REFERENCES		
[SUPPLEMENT]	OBSERVED DATA LIST, ANALIZED CURVE BY RESISTIVITY LAYERS MODEL APPENDED MAPS	

LIST OF ILLUSTRATION

Fig.1	Location Map of Project Area
Fig.2	Location Map of Survey Area (1)
Fig.I-1	Aerial photograph compilation of the Surface Geology TYNAN CLAIMS
Fig.I-2	Geological Map of Area C
Fig.I-3	Geological Map of Area D1
Fig.I-4	Geological Map of Area D2, D3
Fig.II-1	Location Map of Survey Area (2)
Fig.II-2	CSAMT Measurement
Fig.II-3	Schematic Diagram of CSAMT Measurement
Fig.II-4	Representative Families of Curves for Various Depths to the Bottom of the First Layer and Various Range
Fig.II-5	Analytical Curve of CSAMT
Fig.II-6	Schematic CSAMT Curve
Fig.II-7	Plan of Apparent Resistivity (Area C, 1024 Hz)
Fig.II-8	Plan of Apparent Resistivity (Area C, 256 Hz)
Fig.II-9	Plan of Apparent Resistivity (Area C, 64 Hz)
Fig.II-10	Plan of Apparent Resistivity (Area D1, 1024 Hz)
Fig.II-11	Plan of Apparent Resistivity (Area D1, 256 Hz)
Fig.II-12	Plan of Apparent Resistivity (Area D1, 64 Hz)
Fig.II-13	Plan of Apparent Resistivity (Area D2, D3, 1024 Hz)
Fig.II-14	Plan of Apparent Resistivity (Area D2, D3, 256 Hz)
Fig.II-15	Plan of Apparent Resistivity (Area D2, D3, 64 Hz)
Fig.II-16	Section of Apparent Resistivity (Line D-7)
Fig.II-17	Section of Apparent Resistivity (Line D-4)
Fig.II-18	Section of Apparent Resistivity (Line D-37)
Fig.II-19	Section of Apparent Resistivity (Line D-30)
Fig.II-20	Plan of Resistivity Structure (Area C)
Fig.II-21	Plan of Resistivity Structure (Area C)
Fig.II-22	Plan of Resistivity Structure (Area D1)
Fig.II-23	Plan of Resistivity Structure (Area D1)
Fig.II-24	Plan of Resistivity Structure (Area D2, D3)
Fig.II-25	Plan of Resistivity Structure (Area D2, D3)

Fig.II-26	Section of Resistivity Structure (Line D-30)
Fig.II-27	Section of Resistivity Structure (Line D-37)
Fig.II-28	Section of Resistivity Structure (Line D-4)
Fig.II-29	Section of Resistivity Structure (Line D-7)
Fig.II-30	Block Diagram of Spectral IP Survey Instrument
Fig.II-31	Layout of Potential Electrodes and Preamplifier
Fig.II-32	Concept of Spectral IP
Fig.II-33	Transmitted Waveform and Received Waveform
Fig.II-34	Relationship between Frequency Effect and Phase Angle
Fig.II-35	Block Diagram of Laboratory Measurement
Fig.II-36	Phase Spectral of Rocks Samples
Fig.II-37(a)	Location of SIP Survey Lines
(b)	Section of Line A
Fig.II-38	Spectral IP Pseudo-Section Line A(Trojan Mine)
Fig.II-39-1	Spectral IP Pseudo-Section of Line A (1)
Fig.II-39-2	Spectral IP Pseudo-Section of Line A (2)
Fig.II-39-3	Spectral IP Pseudo-Section of Line A (3)
Fig.II-40-1	Spectral IP Pseudo-Section of Line B (1)
Fig.II-40-2	Spectral IP Pseudo-Section of Line B (2)
Fig.II-40-3	Spectral IP Pseudo-Section of Line B (3)
Fig.II-41-1	Spectral IP Pseudo-Section of Line C (1)
Fig.II-41-2	Spectral IP Pseudo-Section of Line C (2)
Fig.II-41-3	Spectral IP Pseudo-Section of Line C (3)
Fig.II-42-1	Spectral IP Pseudo-Section of Line D (1)
Fig.II-42-2	Spectral IP Pseudo-Section of Line D (2)
Fig.II-42-3	Spectral IP Pseudo-Section of Line D (3)
Fig.II-43-1	Spectrum Diagram of Line A (1)
Fig.II-43-2	Spectrum Diagram of Line A (2)
Fig.II-44-1	Spectrum Diagram of Line B (1)
Fig.II-44-2	Spectrum Diagram of Line B (2)
Fig.II-45-1	Spectrum Diagram of Line C (1)
Fig.II-45-2	Spectrum Diagram of Line C (2)
Fig.II-46-1	Spectrum Diagram of Line D (1)
Fig.II-46-2	Spectrum Diagram of Line D (2)
Fig.III-1	Compilation Map of 'GSAMT, SIP Results, Geology & Geochemistry

LIST OF TABLES

Table.II-1	Geophysical Survey Plan
Table.II-2	Outline of Field Survey
Table.II-3	Table of Skin Depth
Table.II-4	CSAMT Survey Instruments
Table.II-5	Spectral IP Survey Instruments
Table.II-6	IP Properties of Ore and Rock Sample
Table.II-7	Calculating method of Real Part, Imaginary Part

PART 1
GENERAL DESCRIPTION

CHAPTER 1. INTRODUCTION

1-1 Purpose of the Survey

The purpose of this project was to evaluate the geological setting and potential for mineral resources in the project area.

Four blocks, Area C, D-1, D-2, D-3, of 21km² total area, were selected from the results of the first year survey program for a second year investigation program applying modern geophysical methods, Controlled-Source Audio-Magnetotelluric (CSAMT) and Spectral Induced Polarization (SIP).

The principal purpose of the second year program was to examine the possibility of the existence of mineralized zones in the area by finding geophysical anomalies and determining their properties.

1-2 Outline of the Survey

The survey program was conducted from July 6 to November 19, 1984.

As an initial program, a CSAMT survey was conducted to detect low resistivity zones favourable for hosting some conductive sulphide minerals. During the next stage, a SIP Survey was conducted to follow up the low resistivity zones by finding IP anomalies.

Three hundred and six points were measured in the CSAMT survey, and, in the SIP survey, 10km survey lines with 300 survey points were measured.

Laboratory SIP test work was conducted in Japan after the completion of the field work on 22 typical rock specimens taken from the survey area.

The survey work was done by the team with the cooperation of the Geological Survey Department of the Ministry of Mines of Zimbabwe which dispatched a geophysicist and geophysical technician to the team.

1-3 Organization of the Survey Team

The members who were involved in the planning, managing, and field survey were as follows.

(1) Planning and Managing

Japanese Members

Ken NAKAYAMA	Metal Mining Agency of Japan
Takahisa YAMAMOTO	Metal Mining Agency of Japan
Tadaaki EZAWA	Metal Mining Agency of Japan
Yosuke SUZUKI	Metal Mining Agency of Japan

Zimbabwean Members

E.R. MORRISON	Geological Survey Department
D.E.H. MURANGARI	Geological Survey Department
C.B. ANDERSON	Geological Survey Department

(2) Field Survey Team

Japanese Members

Akiyoshi KOMURA	Leader, Dowa Koei Co., Ltd.
Yasuo ENDO	Member, Dowa Koei Co., Ltd.
Toshiie TSUBAKITA	Member, Dowa Koei Co., Ltd.

Zimbabwean Members

Peter ZHOU	Geological Survey Department
Mabasa HAWADI	Geological Survey Department

CHAPTER 2. GENERAL CIRCUMSTANCES OF THE SURVEY AREA

2-1 Location and Transportation

The survey area is located 14km to 25km southeast of Bindura which is 70km northeast of the capital city, Harare. It takes about one hour to travel 87km from Harare to Bindura by car on a good highway. A good road network is available from Bindura to the survey area, although some parts are dirt roads. From Bindura, it takes about 20 minutes to Area D-1, and 40 minutes to Area C.

2-2 Topography and Climate

The survey area is located in the Southern African Plateau at an altitude of 1,000 to 1,200m above sea level. Topography well reflects the geology. Andesitic to basaltic lavas, serpentines, and banded ironstones are found in the area which features significant elongated narrow mountain ranges rising 200 to 300m from the background areas. The surrounding, flat, areas are suitable for farming. In the mountain ranges, scarce shrubs grow. Granite-gneiss complexes are found associated with rounded hills in significant contrast to the former region where the survey area is mainly located.

The climate of the survey area is not tropical because of the high altitude, despite the latitude of 17° south. Seasons are clearly divided into two, dry from April to October and wet from November to March. Precipitation per year is usually 700 to 900mm. This year's survey work was done in the dry season, when the temperature was 25° to 30° in the day time, and below 15° at night. October is the hottest month of the year, and the temperature never fell below 30° day and night for several days. In November, the climate changed very suddenly. It rained almost every

afternoon, and the temperature fell to about 18° in the day time. 1984 was expected to have normal rainfall.

2-3 General Social Circumstances

Four years have passed since independence in 1980. The society has been changing toward socialization, and the departure of white people is continuing (at present only 70,000 still remain in the country). The international trade balance is becoming serious as a result of the world wide recession and three year's drought. Inflation is accelerating, and the value of the Zimbabwean Dollar quickly declining (as of November 1984 Z\$1= US\$0.7). The government is endeavouring to improve the situation.

CHAPTER 3. GENERAL AND ECONOMIC GEOLOGY

3-1 General Geology

The land of Zimbabwe is geologically divided into two parts, the Rhodesian Craton area occupying the central eastern part of the country and the rest of the younger geological terrane occupying the northwestern and southeastern parts of the country. The Rhodesian Craton is one of the oldest archean cratons in the world (3.6 b.y. to 2.4 b.y.), and consists of granitic and gneissic terrane containing several greenstone belts. The greenstone belts consist mainly of intermediate to mafic lavas and pyroclastics, and various sedimentary piles, and these rocks are metamorphosed to the green-rock phase. The stratigraphy of these belts is as follows.

Shamvaian Group	clayey to pebbly sedimentary rock piles, felsic pyroclastic rock piles.
Bulawayan Group	
Upper Bulawayan Formation	intermediate to mafic lavas and pyro- clastic rock piles; ultramafic komatiitic lavas, thin layers of cherts, limestones, and banded-ironstones.
Lower Bulawayan Formation	mafic lavas, cherts, conglomerates, phyllites, and banded ironstones.
Sebakwian Group	Intermediate to mafic lavas and pyro- clastic rock piles, thin layers of cherts, limestones, and banded ironstones.

The Rhodesian Craton is surrounded by the Zambezi Mobile Belt to the north, the Mozambique Mobile Belt to the east, and the Limpopo Mobile Belt to the south. These mobile belts are of proterozoic activity (550 m.y.).

In the central part of this country, a very peculiar geological feature,

the Great Dyke, extends about 540km north to south. Its activity age is 2.5 b.y. The rocks of this dyke are mafic to ultramafic layered differentiated rocks.

The survey area is located in the Shamva Grenstone Belt, one of the country's greenstone belts, and consists mainly of intermediate to mafic lavas and pyroclastic rock piles, komatiitic lavas, banded ironstones, cherts, limestones, and sandstones of the Upper Bulawayan Formation.

To the west and south of the survey area, granitic-gneissic rock terrane, believed to be reactivated igneous intrusions into the greenstone belts in most of the regions, is located.

This year's survey areas were selected, on the basis of the results of the first year's geological and geochemical survey programs, where extensive serpentine intrusives are distributed. These serpentines are parts of ultramafic activities which belong to komatiitic rock series, and usually contain more than 35% MgO. Komatiitic lavas sometimes show remarkable spinifex texture, and are easily determined.

The geological structure in the southern part of the survey areas, D-2 and D-3, is controlled by the distribution pattern of the granitic complex body surrounding the greenstone belt, and some significant tectonic features, such as faults, are located there. Therefore, its geological structure is very complicated. The dips of the formations and other features such as intrusive bodies of the serpentines seem to be close to vertical.

3-2 Economic Geology

Ore deposits distributed in the survey area are as follows.

(1) Gold Deposits

Shamva Deposit, Gold Deposits around the Bindura Granite (Kimberley Reef, R.A.N., Kingsley Hoard, Prince of Wales, Slam, Promoter, Hay,

etc.), Montdor Deposit, Red Dragon Deposit, Churchill Deposit, Ivan Zone, Inyagui Deposit, Kadangi Deposit

(2) Nickel Deposits

Trojan Deposit, Katio Occurrence, Tynan Occurrence

(3) Pegmatite Deposits

Uzumba Deposit, Zero Deposit, Wanroo Deposit, Look and Weep Deposit, Chenjera Deposit, Tafuna Hill Deposit, Robnik Deposit, Mejenzi Deposit, Dale 4 Deposit, Nyagui Deposit, Lochness Deposit, Nkanga Deposit

Among them, Shamva Gold Mine, R.A.N. Gold Mine, and Trojan Nickel Mine are operating at present. Their production scales are as follows. (data of 1983)

Shamva Gold Mine

Gold produced per year	540 kg
Ore mined per year	150,000 ton
Grade	4.5 g/t

R.A.N. Gold Mine

No published data available, but its scale is very small.

Trojan Nickel Mine

Nickel Produced per year	3,025 ton
Ore mined per year	746,000 ton
Grade	0.55% Ni

Trojan Nickel Ore Deposits located to the west of the survey area are closely associated with komatiitic ultramafic rocks which are in the Upper Bulawayan Formation. It is a well known fact that nickel ore deposits associated with such komatiitic ultramafic rocks have very high nickel/copper ratio (7:1 to 16:1) compared with those associated with tholeiitic ultramafic rocks which have relatively low nickel/copper ratio (1:1 to 2:1).

In the survey area, the lower parts of the Upper Bulawayan Formation which are the host horizon of the Trojan ore deposits extend from the Trojan area, and such komatiitic ultramafic rocks are well distributed. Judging from the good geological setting, the potential for similar types of nickel ore deposits is high.

Two mineral occurrences, Tynan Nickel Mineralized Zone and Lochness Tin-bearing Pegmatite, are located in this year's survey areas.

Tynan Nickel Occurrence

The occurrence is located in Area D-3, and is of a nickel mineralized zone associated with serpentine bodies intruded into graphitic sediments, banded ironstones, komatiitic lavas, and andesitic lavas and pyroclastics. This zone is located on our geophysical survey lines D-10-39 to D-9-42.

This mineralized zone was previously owned by several companies such as Rio Tinto, Anglo Vaal, J.C.I., Blanket Mines, Prospecting Ventures (A.A.C.), Tynan Syndicate, etc. They all conducted extensive exploration activities, including geological, geochemical, trenching, and drilling surveys. Among them, Blanket Mines was the most active, and conducted a significant drilling program including ten drill holes in 1975, but failed to find economic ore deposits. A plan map of this property, made by Blanket Mines, is shown in Fig. I-1.

Our geophysical survey lines covered this zone, and the CSAMT survey revealed a low resistivity area coincident with it, but the SIP survey lines were set up about 600m to 800m to the south.

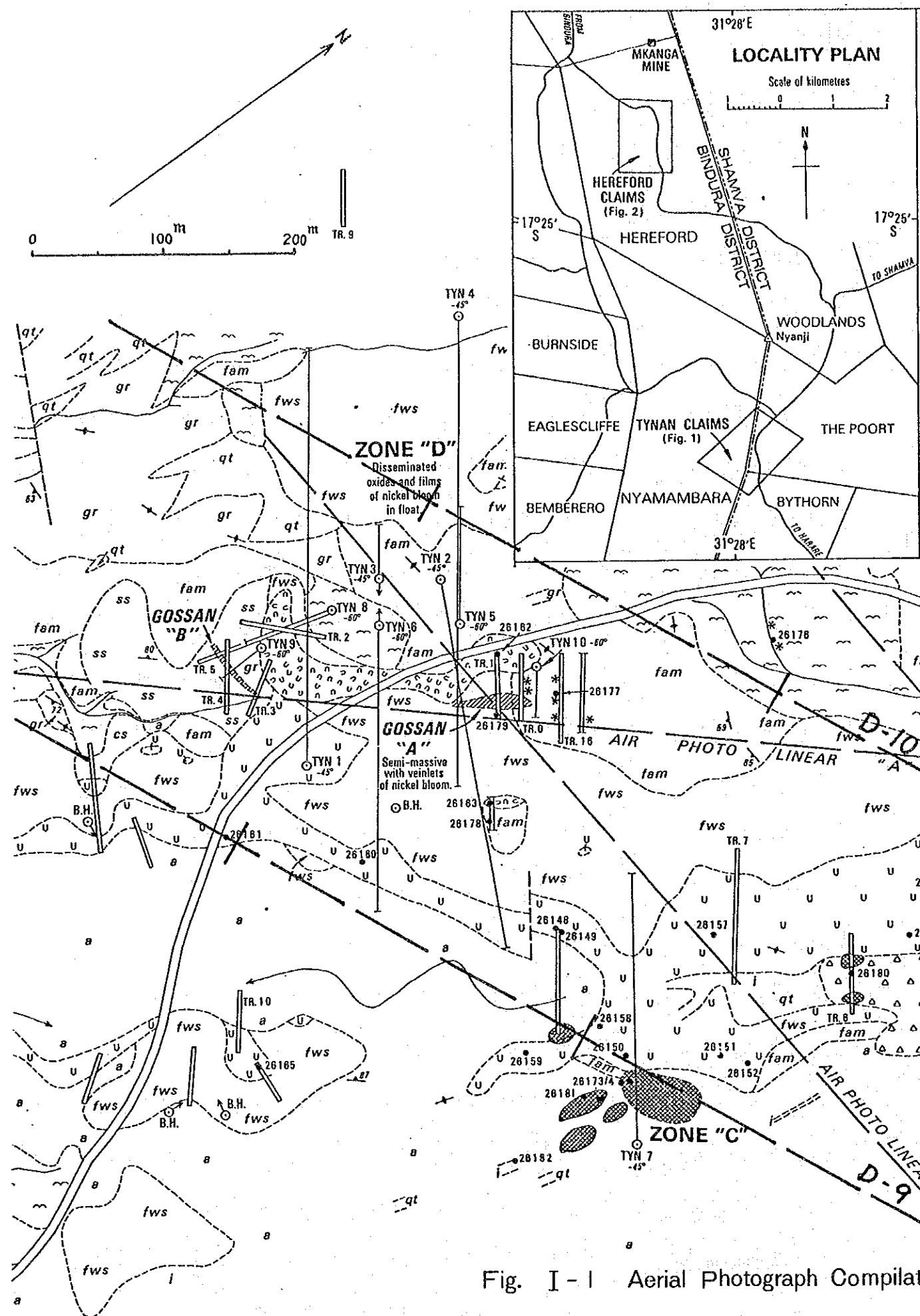
Lochness Tin-bearing Pegmatite

The pegmatite dyke is located in the north-central part of Area D-1, and our geophysical survey lines D-39-6 to D-38-6 extended along the top ridge of north-south low hilly range. It intrudes into a serpentine body and contains large crystals of quartz and feldspar, large amounts of mica,

and some black, pale green, and pinkish tourmaline crystals.

An old working exists at the northern end of the pegmatite, but it is small (about 20m long, 2m wide, and several meters deep), judging from the amount of the waste dump. It is very hard to find cassiterite crystals in the waste.

About 300m to the north, similar type and scale pegmatite dyke is located on the survey lines D-40-6 to D-41-6, but old working was not seen there.



EXPLANATION

- Alluvium or soil cover
 - Talus
 - Gossan
 - Microgranite with lepidolite greissen
 - ULTRAMAFIC SUITE**
 - Massive to weakly sheared, fine-grained translucent serpentinite (*ms Unit*)
 - Weathered ferruginous (*jaspery*) serpentinite
 - Spotted serpentinite
 - Massive serpentinitized dunite (*sdt Unit*)
 - MAFIC SUITE**
 - Sheared chloritic greenstone
 - Fibrous amphibolite-a contact alteration of the chloritic greenstones
 - Fine-grained chlorite schist
 - SEDIMENTARY SUITE**
 - Black graphitic argillite
 - Sulphidic argillite
 - Arkose and greywacke
 - Fine-grained, fractured quartzite
 - Ironstone gossan, sometimes fractured
 - Geological contact
 - Fault or fracture
 - Foliation, strike and dip
 - Foliation, where vertical
 - Blanket Mines Borehole with inclination
 - Trench
 - Stream - course
- Additions by L. Haynes, 1983.
- Gossan
 - Spinifex texture seen
 - Early borehole with direction of inclination
 - Trench
 - 26183 Sampling point and Geological Survey collection number

SHAMVA AND BINDURA DISTRICTS
 Modified by L. Haynes
 from a compilation by N.J.G. Graham for Blanket Mines (Pvt.) Ltd., 1975.

Fig. I - I Aerial Photograph Compilation of the Surface Geology TYNAN CLAIMS

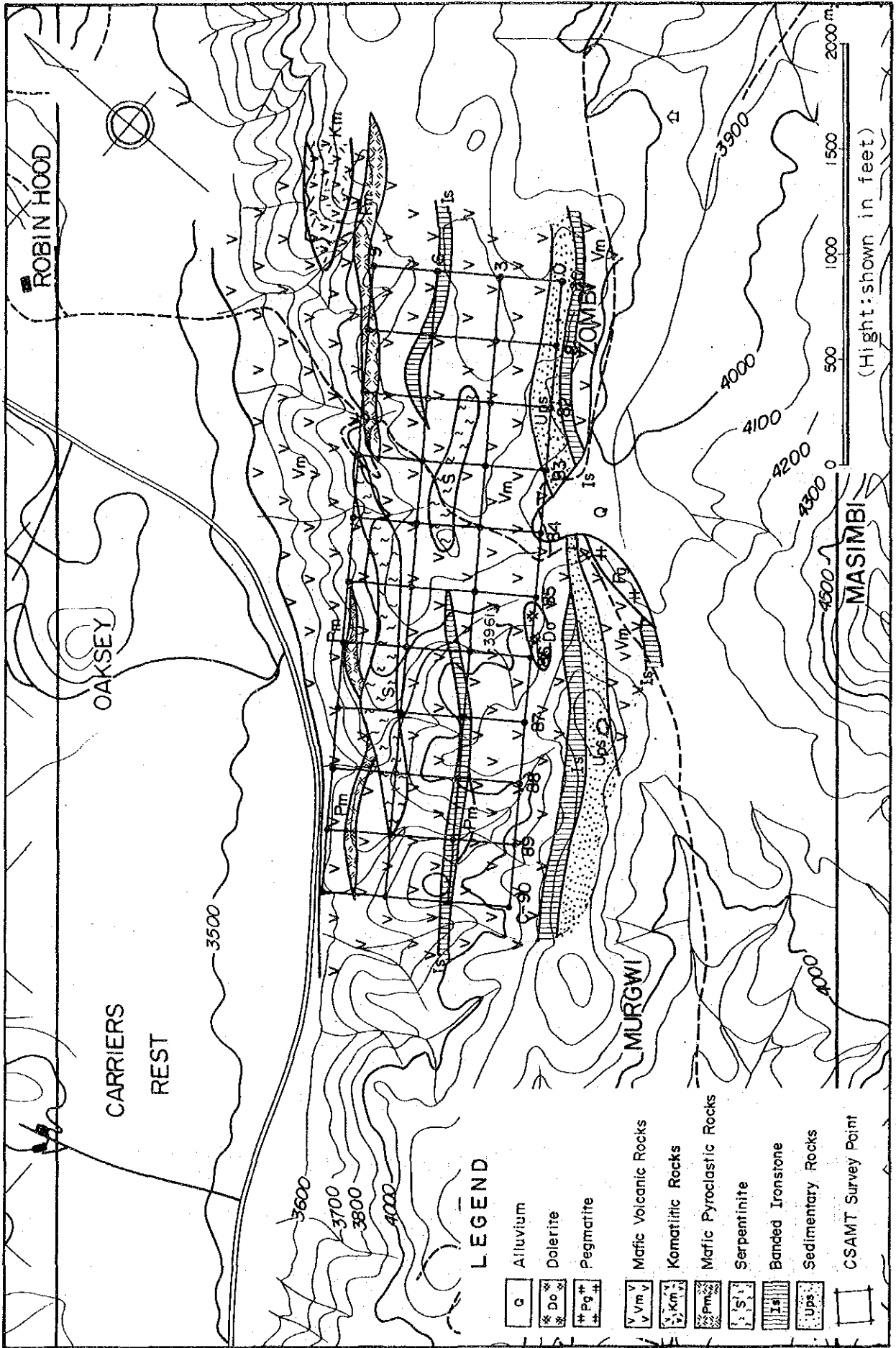


Fig. I-2 Geological Map of Area C

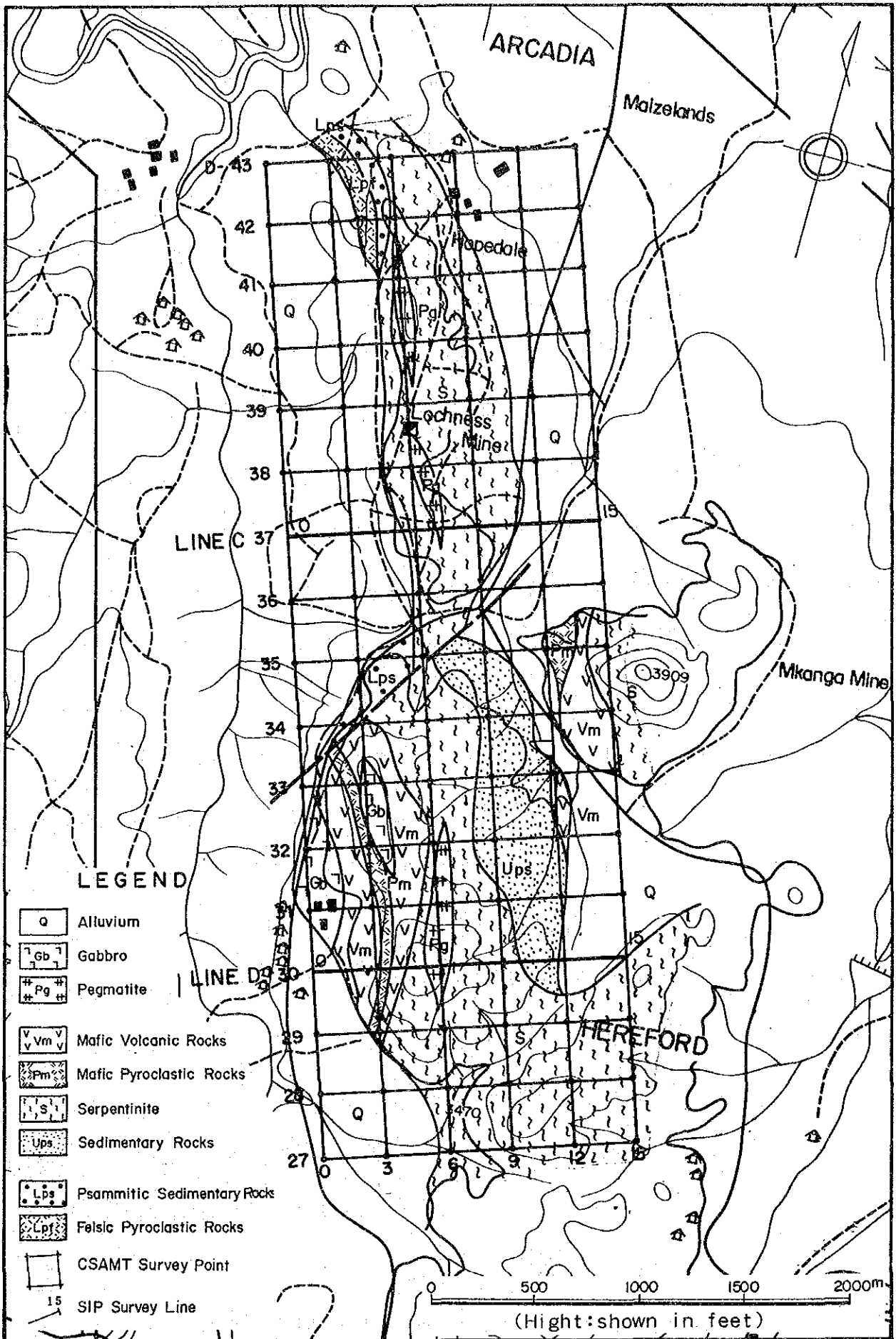
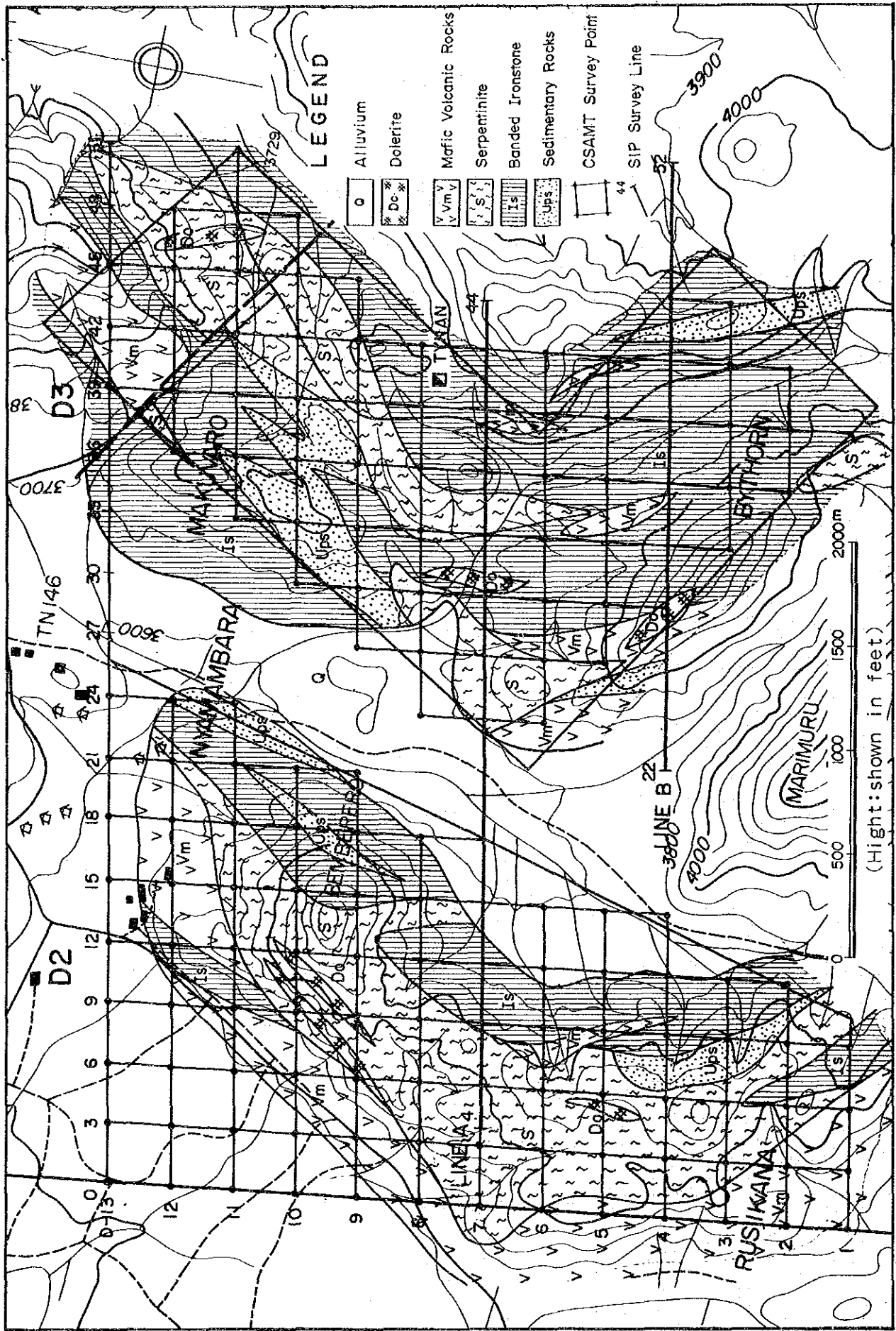


Fig. I - 3 Geological Map of Area D I



PART 2
GEOPHYSICAL SURVEY

CHAPTER 1. OUTLINE OF THE SURVEY

1-1 Survey Plan

We planned the SIP survey on the basis of CSAMT survey results, see Fig. 3.

We also planned to collect representative rocks and minerals in the survey areas for laboratory SIP tests, using the same frequencies as in the field measurements.

Survey plans for this year are as shown in Table II-1.

Table II-1 Geophysical Survey Plan

(Field Work)

Method	Area	Plan
CSAMT	Area C	Area : 2.7 km ² Survey Point : 44
	Area D	Area : 18.3 km ² Survey Point : 260
SIP	Area C and D	Survey Line Length : 10.0 km Survey Point : 300

(Laboratory Work)

Item	No. of Samples
Laboratory SIP Sample Test	20

1-2 Survey Method

The CSAMT method measures electromagnetic fields in a frequency band from about 1 Hz to several kHz. It is superior to the IP method because linear survey lines are not required and movement of current electrodes is small. It is also able to find low resistivity zones, resulting from

mineralized zones, altered zones etc. quickly, and is therefore often used in geothermal exploration as a reconnaissance exploration method over areas.

The SIP method measures potential differences (magnitudes) and phase differences (phases) using many frequencies from 0.125 to 88 Hz to determine IP effects as spectral characteristics.

1-3 Survey Records and Efficiency

This year's field survey records are shown in Table II-2.

Table II-2 Outline of Geophysical Survey Schedule

Method	Area	Period	Days	Survey Line Length (km)	No. of Survey Points	Note	
CSAMT	C	Sept., 30 ~ Oct., 6	14		71	<ul style="list-style-type: none"> • Days include Line Survey and setting days • Efficiency 5.4 points/day (306 points/57 days) • Due to damage of the equipment, an engineer was invited from Zonge to fix up. Start of the actual survey was delayed by about one month 	
	D	D1	Sept., 16 ~ Sept., 29	22			89
		D2	Aug., 25 ~ Sept., 15	14			102
		D3	Aug., 11 ~ Aug., 24	7			44
	Total			57			306
SIP	Line A	Oct., 17 ~ Oct., 29	13	4.0	160	<ul style="list-style-type: none"> • Days include Line Survey and setting days • Efficiency 11.5 points/day (300 points/26 days) 	
	Line B	Oct., 30 ~ Nov., 5	7	3.0	80		
	Line C	Nov., 6 ~ Nov., 8	3	1.5	30		
	Line D	Nov., 9 ~ Nov., 11	3	1.5	30		
	Total			26	10.0		300

CHAPTER 2. CSAMT SURVEY

2-1 Survey Method

2-1-1 Measuring Method

CSAMT measuring systems used in this survey are shown in Fig. II-2. The transmission frequencies were 4, 8, 16, 32, 64, 128, 256, 512, 1024 and 2048 Hz, (ten in total).

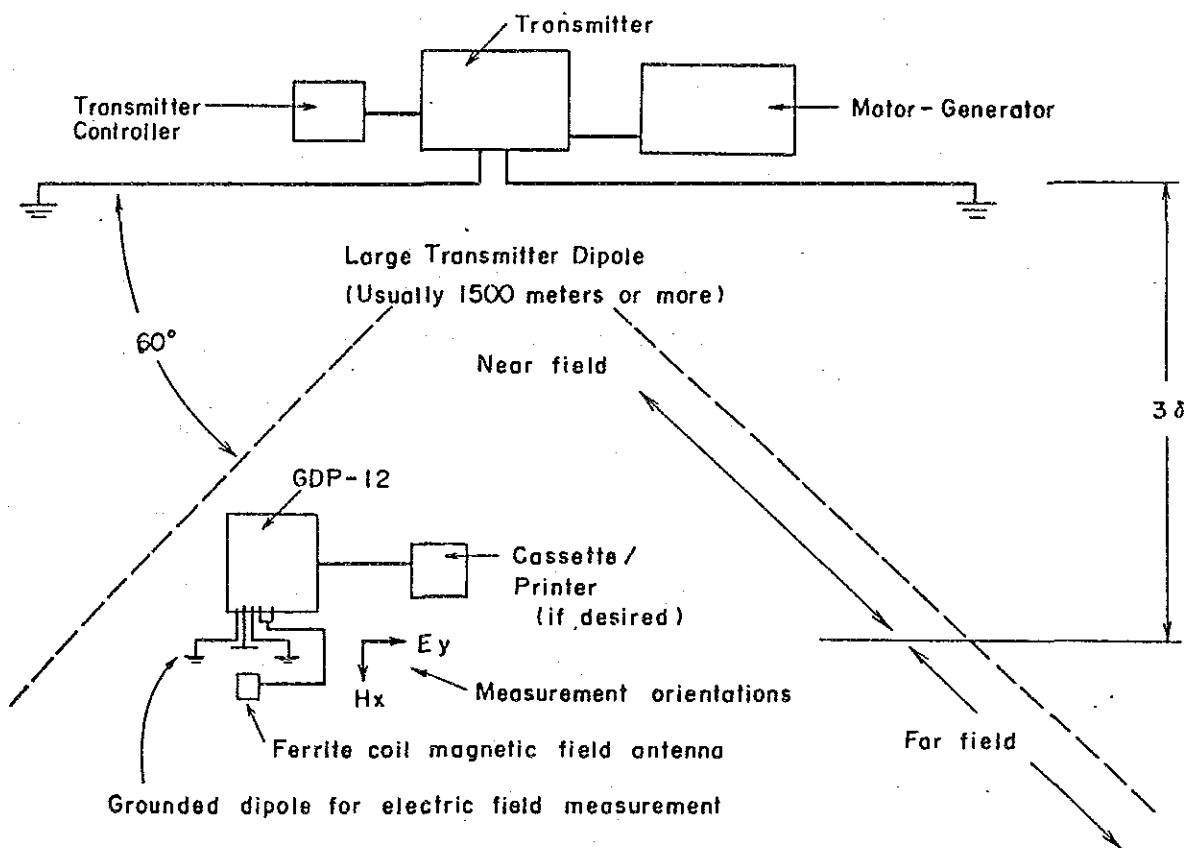


Fig. II - 2 CSAMT Geometry

Measured components were the electric field (E), parallel to the connection between two current electrodes, and the magnetic field (H), perpendicular to the electric field. Signals from both electric and magnetic fields were processed by a receiver (GDP-12) which outputs apparent

resistivity (ρ_a) and phase difference (PD), between the magnetic field and the electric field.

Distances between transmitter and receiver must be more than three times the "skin depth" at which an assumption of plane electromagnetic waves is approximately valid (usually 5 - 10 km).

Skin depth is given by the following equation:

$$\delta = 503 \sqrt{\frac{\rho}{f}} \quad (\text{m})$$

where δ : skin depth (m)

ρ : resistivity ($\Omega\text{-m}$)

f : frequency (the lowest frequency used in measurement, which is 4 Hz in this case)

Skin depths of a semi-infinite homogeneous medium, calculated using the above equation, and their relationships with various parameters are shown in Table II-3. Skin depth increases with lower transmission frequencies and higher resistivity of the medium.

Table II-3 Table of Skin Depth

Note : Skin Depth (m) = $503 \times \sqrt{\rho/f}$

		RESISTIVITY IN OHM-METERS												
		5	10	20	40	80	160	320	640	1,280	2,560			
FREQUENCY	<u>f Hz</u>											<u>f Hz</u>		
	2048	25	35	50	70	99	141	199	281	398	562	795	1,024	2,048
	1,024	35	50	70	99	141	199	281	398	562	795	1,024	2,048	
	512	50	70	99	141	199	281	398	562	795	1,124	1,591	2,249	3,181
	256	70	99	141	199	281	398	562	795	1,124	1,591	2,249	3,181	4,499
	128	99	141	199	281	398	562	795	1,124	1,591	2,249	3,181	4,499	6,362
	64	141	199	281	398	562	795	1,124	1,591	2,249	3,181	4,499	6,362	8,998
	32	199	281	398	562	795	1,124	1,591	2,249	3,181	4,499	6,362	8,998	12,725
	16	281	398	562	795	1,124	1,591	2,249	3,181	4,499	6,362	8,998	12,725	17,453
	8	398	562	795	1,124	1,591	2,249	3,181	4,499	6,362	8,998	12,725	17,453	24,000
	4	562	795	1,124	1,591	2,249	3,181	4,499	6,362	8,998	12,725	17,453	24,000	32,000

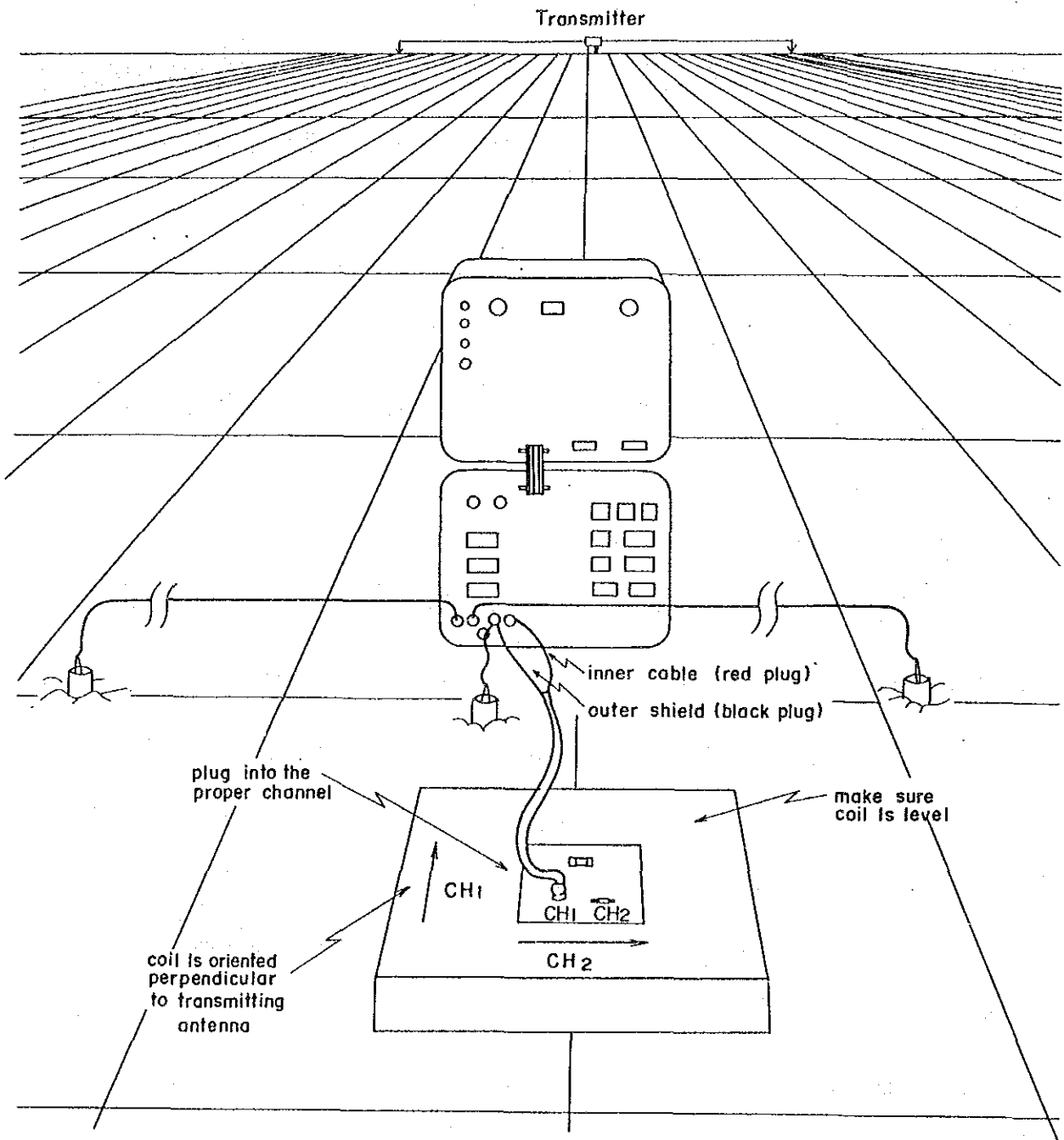


Fig. I - 3 Schematic Diagram of CSAMT Measurement

Table II - 4 CSAMT Survey Instruments

System	Equipment	Specification	Number
Transmitter System	Zonge, Inc. Model GGT-20 Transmitter	Output Voltage: 400 V ~ 800 V Output Current: 0.2 A ~ 25 A Output Wave Form: Rectangular Output Current Frequency: 1/1024 Hz ~ 2048 Hz Weight: 113 kg	1
	Model XMT-12 Transmitter Controller	Control Current Frequency: 1/1024 Hz ~ 2048 Hz Weight: 5.8 kg Power Source: 12 V Battery	1
	Model VR-1 Voltage Regulator	Weight: 3.7 kg	1
	Model 2MG-10 Engine-Generator	Maximum Output Power: 10 KW Frequency: 400 Hz Rating Voltage: 115 V Engine: 23 Hp, 2 Cylinder, Aircooling	1
Receiver System	Model GDP-12 Receiver	Input Signal: 2 channels AMT Receiving Frequency: 0.5 Hz ~ 2048 Hz (13 kinds) Receiving Voltage Sensitivity: 0.2 μ V Weight: 15 kg Power Source: 12 V Battery	1
	Model CAP-12 Mini Cassette Recorder	Weight: 6.2 kg Power Source: 12 V Battery	
	Techtronics Model 212 Oscilloscope		1
	AMT Antenna	Weight: 9.8 kg Power Source: 9 V Transistor Battery	1
Electrode	Current Electrode	Iron Rod: ϕ 16 mm, Length 80 cm Copper Net	200 50
	Potential Electrode	Saturated Copper Sulphate Solution Non Polarized Electrode	10
Wire	Fujikura Electric Kyosan Electric	VSF \times 1.25 mm ² Vinyl Wire CVV ₁ \times 3.5 mm ² Vinyl Wire	1000 m 6000 m
Survey Equipment	Ushikata Pocket Compass 100 m Eslon Tape		2
Transceiver	Sony	Output Power: 500 mW	6

Although measurements of the field between the broken lines (shown in Fig. II-2) are possible, at less than 36, it is a near field and analysis becomes difficult. Measurement of this field was avoided.

Current electrodes were installed, as far as possible where earth resistance could be reduced. The transmitter system was installed at any easy access place between the two electrodes. Although transmission currents varied between each of the No. 1 to No. 4 current electrodes, current from 3A to 11A was transmitted through the earth. There was also a place where high frequency current was reduced to a minimum of 5A.

Layout of the receiver system is shown in Fig. II-3. Three copper-copper sulfate electrodes and a high sensitivity ferrite coil antenna were connected to a GDP-12 unit. The coil was installed more than 9 m from, and perpendicular to, the center of the electric field dipole (potential electrodes).

The system was installed about 60 m away from automobiles or conductive objects.

2-1-2 Instruments Used

Measuring devices and instruments used in the survey are shown in Table II-4.

2-1-3 Survey Point Positions

Current electrodes were positioned at points, previously selected on a topographical map, 4 km from the area to be measured. They were installed at flat places, 750 m or more apart, right and left of a pre-selected center point.

Fig. 3 shows positions of the current electrodes, and co-ordinates are listed in the separate volume.

Potential electrode survey points were determined by a 300 m grid all over the surveyed area using pocket compasses and measuring ropes (Fig. II-1).

2-2 Data Processing and Analysis

2-2-1 Outline of CSAMT Method

Application of MT (magnetotelluric) methods to geothermal and petroleum exploration has been rapidly developed in the last ten years. The signal source of the method, is the intensity of frequency components of the natural electromagnetic field, which is often unstable above 10 Hz and makes measurement impossible. An artificial signal is therefore generally used when exploring resistivity structures of the ground up to several hundred meters deep.

Goldstein (1971) and Goldstein and Strangway (1975) derived a theoretical equation for surrounding electric and magnetic fields using both-end-earth dipole electric current as an artificial signal source. Water tank and field experiments proved that theory agreed with experimental results. It was shown that observation of electric or magnetic fields, at a survey point approximately three times or more the skin depth from the current source, gave apparent earth resistivity from Cagniard's equation. The equation is also used in common MT methods. Horizontal layer structure, MT method analyzing techniques, can also be utilized. Fig. 7 shows calculating curves for a double layer structure.

Swift's (1971) MT analytical method for a 2-dimensional structure was used as the calculating method.

Sandberg and Hohmann (1982) determined the ground surface apparent resistivity distribution, when a rectangular piece of foreign matter had been buried, by using 3-dimensional model calculations. They named the method CSAMT (Controlled-Source Audiomagnetotelluric Method).

CSAMT is used for observing electromagnetic fields for frequency bands from about 1 Hz to several kHz. CSAMT, together with MT, is used for surveying structures, several hundred meters or more deep, in geothermal and petroleum exploration.

The MT method alone would be inadequate for such surveys CSAMT has a high survey efficiency, requiring a shorter measuring time than the MT method.

Metallic oredeposit exploration requires ground exploration to depths of about 500 m and the CSAMT method also almost matches this requirement.

CSAMT is superior to the IP method, mainly used in metallic ore deposit exploration in the past, because it requires less survey time. Linear survey lines are not required and current electrodes are not moved often. Conversely, it cannot measure IP effect. Therefore, CSAMT is most efficient for finding low resistivity zones of mineralized regions, etc., quickly, over a wide area and then IP or spectral IP methods can be used in detail at such sites.

In this survey, two components, electric field (E_x), parallel to the current dipole, and the magnetic field (H_y), perpendicular to the dipole, were observed at each survey point for ten frequencies ($f = 2,048$ Hz, 1,024 Hz, 512 Hz,, 4 Hz). Apparent resistivity (ρ_a) was calculated using Cagniard's equation:

$$\rho_a = \frac{0.2}{f} \left| \frac{E}{H} \right|^2$$

Underground resistivity structure at each survey point was determined using the MT method horizontal multi-layer structure analysis theory of the apparent resistivity -- frequency ($\rho_a - f$) curve.

2-2-2 Data Processing

The following four observation values are displayed and printed by a GDP-12 receiver.

ME [$\overline{\text{mV}}$ or $\overline{\mu\text{V}}$] received voltage of electric field channel

MH [$\overline{\text{mV}}$ or $\overline{\mu\text{V}}$] received voltage of magnetic field channel

RHO [$\Omega\text{-m}$] apparent resistivity value

PD [radian] phase difference between ME and MH

ME and MH units are $\overline{\text{mV}}$ but in the field notes (appended data), they are noted $\overline{\mu\text{V}}$.

Measured values at each survey point are listed in the separate volume.

Main contents are: "distance between survey point and transmitting source"..... distance between survey point and the center of current electrodes A and B (m).

"electric field" $E[\overline{\text{mV/km}}] = \text{ME}[\overline{\text{mV}}]/50[\text{m}]/1000[\text{km/m}]$

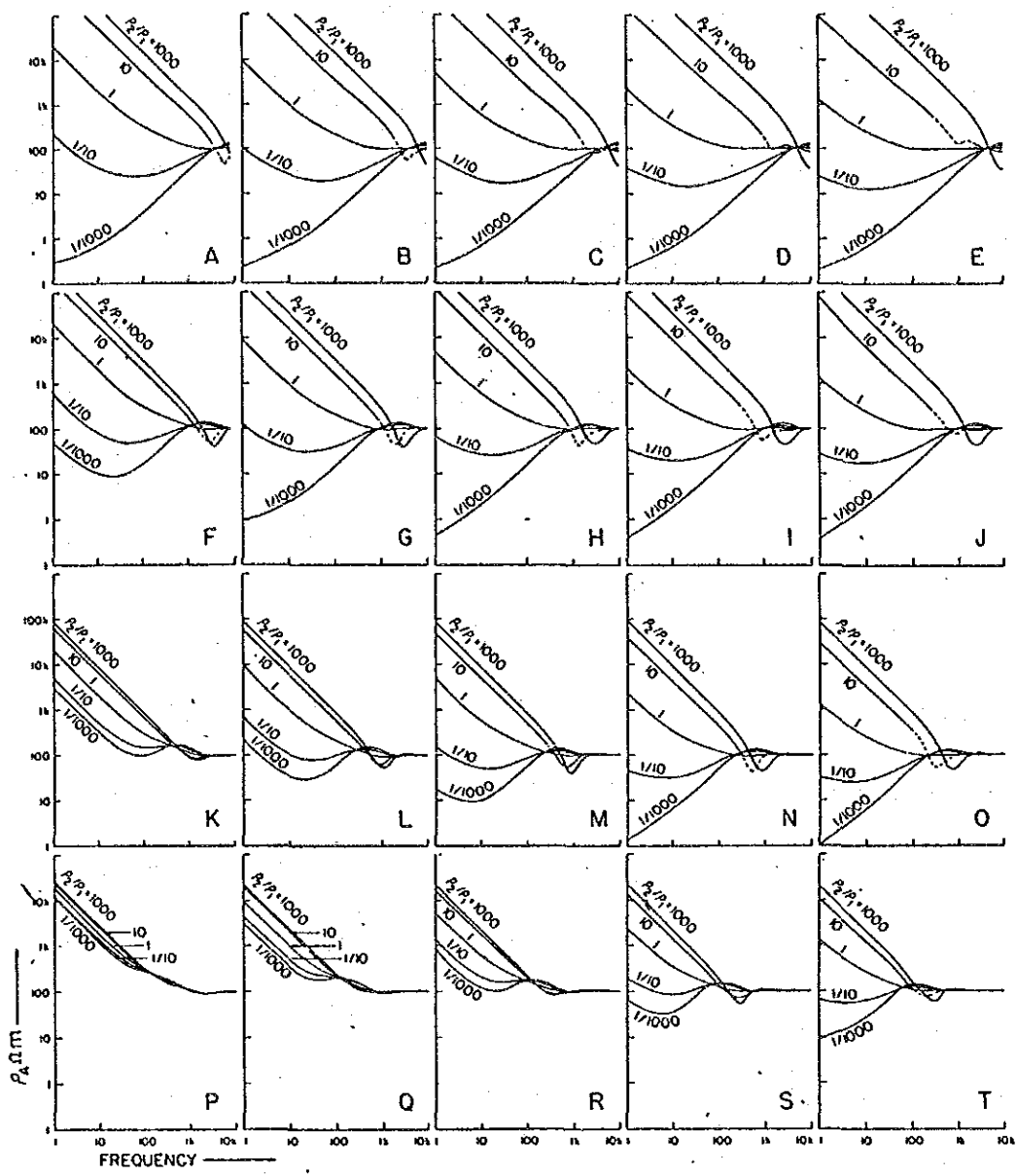
"magnetic field" $H[\text{Gamma}] = \text{ME}[\overline{\text{mV}}]/\text{CG}/\text{CK}(f)$

where CG (coil gain) is the degree of amplification by the built-in magnetic field observing antenna pre-amplifier and CK(f) is an antenna constant, given for each frequency in the calibration table attached to the antenna.

"apparent resistivity" RHO [$\Omega\text{-m}$] The apparent resistivity values are those computed by the microprocessor in the receiver using equation (b-3) mentioned later.

"phase difference" PD [rad] The phase differences are also the values computed in the receiver and displayed.

Mean values of E, H, RHO and PD data were obtained by repeating observations several times for each frequency. Therefore, the values of RHO in the table are slightly different from apparent resistivity values obtained from E, H and equation b-3.



D	R = 500 m	750 m	1,000 m	1,500 m	2,000 m
50 m	A	B	C	D	E
125 m	F	G	H	I	J
250 m	K	L	M	N	O
500 m	P	Q	R	S	T

Fig. II-4 Representatve Families of Curves for Various Depth to the Bottom of First Layer and Various Range

(Goldstein and Strangway, 1975)

The top layer(ρ_1) has a resistivity of 100 Ω -m.

"R" is distance between Tx dipole and receiver point.

Cagniard's equation (1953), derived from the MT method, was used to calculate apparent resistivity (ρ_a [Ω m]),

$$\rho_a = |E_x/H_y|^2 / (2\pi f \mu) \dots\dots\dots (b-1)$$

where E_x is electric field (\bar{V}/m), H_y is magnetic field (A. Turn/m), f is frequency (Hz) and μ is the permeability of vacuum ($4\pi \times 10^{-7}$ H/m).

Hence, equation (b-1) becomes:

$$\rho_a = 1.267 \times 10^5 / f \cdot |E_x/H_y|^2 \dots\dots\dots (b-2)$$

Measured unit values were: [$m\bar{V}/km$] for electric field and [Γ] for magnetic field. Equation (b-3) was used to calculate apparent resistivity.

$$\rho_a = 0.2 / f \cdot |E_x/H_y|^2 \dots\dots\dots (b-3)$$

Observed phase difference values (PD) varied greatly in the range of -7 to +8 radian. As noted in the separate volume, this was inconvenient for discussion of phase difference data. Phase differences between electric and magnetic fields are usually about 45° (0.785 rad) and corrected phase differences in the range -90° to $+90^\circ$ were obtained by adding the appropriate correction to the observed values. Corrected phase differences [rad and degree ($^\circ$)] were added to the separate volume.

Apparent resistivity values (ρ_a) and corrected phase difference (PD-C $^\circ$) often showed steep respective rises and drops. Most of these changes are thought to result from near field effects.

Mean values of apparent resistivity data for each frequency were calculated, and used to draw plane distribution diagrams (scale 1/25000) of apparent resistivity for respective frequencies (Plan of Apparent Resistivity) (Fig.s II-7 to II-15).

Six contour interval values (10, 20, 50, 100, 200 and 500 Ω -m) were determined logarithmically. The geological structure of area C runs NE - SW and that of area D almost N - S so cross-sectional lines in these areas

were selected to cross these directions at right angles.

Apparent resistivity values in the apparent resistivity sectional views (Figs. II-16 to II-19), corresponding to ten frequencies, were plotted in a high to low frequency order. Equi-apparent resistivity curves were then drawn.

Apparent resistivity values show the mean resistivity values corresponding to skin depths, so ordinates and depths do not exactly correspond. These sectional views are therefore, types of pseudosections.

2-2-3. Analytical Methods

CSAMT waves were computed for an arbitrarily given resistivity multi-layer model by a simulation technique using equations (e-1) to (e-6) shown below. This multi-layer model was corrected so that it approximated to the actual CSAMT curves drawn from measured values.

The surface impedance ($Z(0)$) of the $(n+1)$ th layer, for a horizontal multi-layer with resistivity values of respective layers $\rho_1, \rho_2, \dots, \rho_n, \rho_{n+1}$ and depths of respective layers z_1, z_2, \dots, z_n , is shown by the following equation (Reference 9).

$$Z(0) = \frac{E_x}{H_y} \Big|_{z=0} = \frac{i\omega (A_0 + B_0)}{\theta_0 (A_0 - B_0)} \dots\dots\dots (e-1)$$

where,

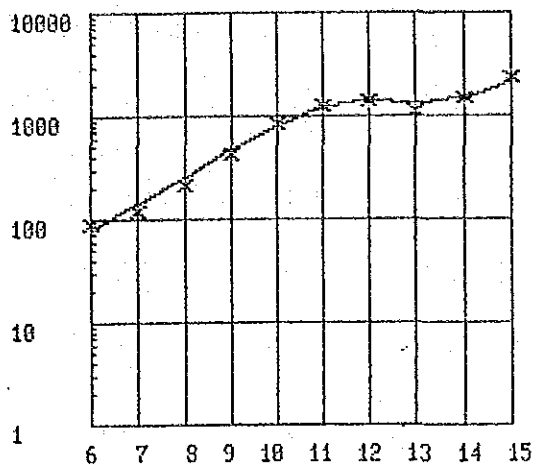
$$A_0 + B_0 = A_1 + B_1 \dots\dots\dots (e-2)$$

$$\theta_0 (A_0 - B_0) = \theta_1 (A_1 + B_1)$$

$$A_j \exp(-\theta_j z_j) + B_j \exp(\theta_j z_j) = A_{j+1} \exp(\theta_{j+1} z_j) + B_{j+1} \exp(\theta_{j+1} z_j) \dots\dots (e-3)$$

$$= \theta_{j+1} [A_{j+1} \exp(-\theta_{j+1} z_j) - B_{j+1} \exp(\theta_{j+1} z_j)]$$

(j = 1, 2, \dots, n)



Station No. = D-12-42

	Rho (ohm)	Depth (m)
1	3200	300
2	500	600
3	2500	1300
4		5

F	OBS	CALC
15	2331.3	2085.8
14	1474.5	1498.8
13	1140.0	1359.0
12	1420.3	1432.7
11	1245.5	1244.6
10	834.2	816.3
9	433.4	464.0
8	212.3	255.3
7	116.0	141.1
6	87.3	80.2

Fig. II-5 Analytical Curve of CSAMT (No. D-12-42)

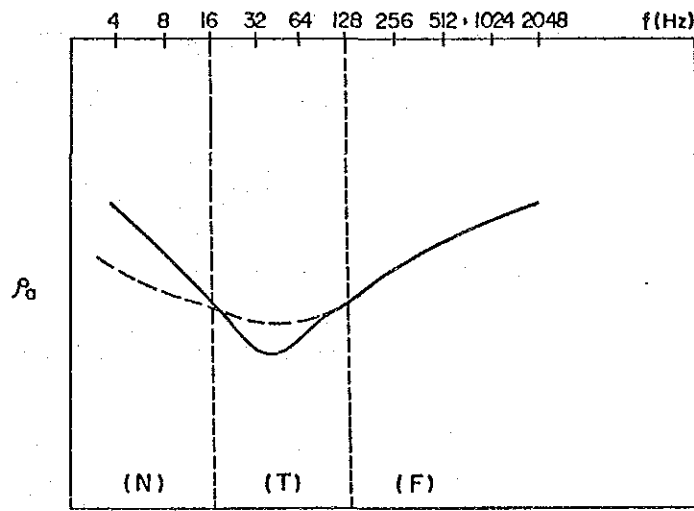


Fig. II-6 Schematic CSAMT Curve

- (F) : far-field data
- (T) : transition-zone
- (N) : near-field data

The dashed line give the Calculated Curve
 (Zonge, Inc. Interpretation Guide for CSAMT Data, 1982)

$$\begin{aligned}
 A_n &= \frac{\theta_{n+1} + \theta_n}{2\theta_n} \exp [-(\theta_{n+1} - \theta_n) zn] \\
 B_n &= \frac{\theta_{n+1} - \theta_n}{2\theta_n} \exp [-(\theta_{n+1} + \theta_n) zn]
 \end{aligned}
 \dots\dots\dots (e-4)$$

where the cgsemu unit system is used and θ shows the number of waves.

$$\begin{aligned}
 \theta_j &= \left(\frac{4\pi i \omega}{\rho_j} \right)^{1/2} \quad (j = 1, 2, \dots, n) \\
 \omega &= 2\pi f
 \end{aligned}$$

However, because $1 \text{ m}\bar{V}/\text{km} = 1 \text{ emu}$, $1 \Omega\text{m} = 10^{11} \text{ emu}$ and $1\text{Y} = 10^{-5} \text{ emu}$, the apparent resistivity equation (b-3) can be represented in the cgsemu unit system as:

$$\rho_a = \frac{2}{f} |Z(0)|^2 \text{ (e.m.u.)} \dots\dots\dots (e-5)$$

Accordingly, apparent resistivity (ρ_a) can be determined from equations (e-1) to (e-4) and (e-5), and the equation for calculating ρ_a in Ωm units becomes as follows.

$$\rho_a = \frac{2}{f} |Z(0)|^2 / 10^{11} \text{ } [\Omega\text{-m}] \dots\dots\dots (e-6)$$

Actual simulation was carried out by displaying theoretical and measured curves simultaneously on a personal computer. The curves were matched visually by trial-and-error manner. Results were output on a graphic printer. An example is shown in Fig. II-5. Bostic Inversion results from the resistivity multi-layer model, were also used.

The CSAMT curves frequently showed three zones, far-field (F), transitional (T) and near field (N) zone as seen in Fig. II-6. Near-field data shows a -45° gradient on the low frequency side of ρ_a -f curves plotted on log-log coordinates.

CSAMT curves, of the two-layer structure model shown in Fig. II-4, had transition zones and near-field zones when the second layer was of high resistivity. These data suggested using a model, having high resistivity

at the lowest layer, for simulation of data including near-field and transition zones. Curve matching was carried out so that computed curves passed the upper part of transition zones and lower part of near-field zones as shown in Fig. II-6.

These simulation analyses gave a total of 306 points which included 40 points of 2-layer structure, 98 points of 3-layer structure and 168 points of 4-layer structure. 1/25000 scale, Plan of Resistivity Structures, were made (Figs. II-20 to II-25) based on the underground resistivity structure at each survey point, obtained by simulation. The figures show the horizontal distributions of underground resistivity at the same depths between survey points. Four depths, 125, 225, 325 and 525-m were selected. Six, logarithmically plotted resistivity contours were selected, (10, 20, 50, 100, 200 and 500 Ω -m) were

Resistivity multi-layer models, obtained by the simulation were plotted in the "Section of Resistivity Structure" (Fig. II-26 to II-28). Resistivity values at respective survey points were connected with solid or broken lines in order to show clearly the distribution of resistivity. These figures are different from the apparent sectional views and show underground resistivity structures. They are displayed on a 1/25000 horizontal scale and a larger vertical one.

2-3 Survey Result and Discussion

2-3-1 Survey Results

Survey results were shown as apparent resistivity plans, apparent resistivity sectional views, resistivity structure plans, and resistivity structure sectional views using methods described in the previous chapter. These results, in combination with the geological and geochemical exploration results from the first year survey, describe each area as follows:

Area C (Figs. II-7 to II-9, Figs. II-20 to II-21)

The apparent resistivity plans show complicated resistivity distributions at shallower depths, but in the deeper part there is a long distribution of low resistivity zones (below 20 Ω -m) running NE to SW through the area to the edge. They extend to the deepest part, although their expansion is unclear. Additionally, low resistivity zones (below 10 Ω -m) of small to medium size were found near survey points C-82-9, C-86-6 and C-89-6.

The resistivity structure plans, show complicated distributions of large resistivity differences in the shallower part (125 m, 225 m depth). Low resistivity zones are distributed near points C-86-0 to C-81-0 at the southern border of the area. They extend from 125 m to 525 m deep. Zones near C-81-0 and C-89-6 go below 125 m. High resistivity zones are distributed near points C-81-3, C-83-3, C-86-3, C-88-3, C-84-9 and C-90-9. Those near survey points C-86-3 and C-88-3 are deeply extended cylindrical shapes.

The low resistivity zones from survey points C-86-0 to C-81-0, near the southern border of the area, did not coincide with geochemical anomalies but there is a possibility of a serpentine extension in the deeper part at survey point C-81-3. A mineralized zone is thought to exist here. The low resistivity zone, near survey point C-89-6, relates to mafic lava and the geochemical anomaly is slightly offset to the eastern side.

Although the low resistivity zone around point C-81-9 was included in the high resistivity zone simulation analysis, it consists of mafic pyroclastic rock and no geochemical anomaly was noticed.

Area D 1 (Figs. II-10 to 12, Figs. II-18 to 19, Figs. II-22 to 23, Figs. II-26 to 27)

The apparent resistivity plans and sectional views, show complicated

resistivity distribution in the shallower part, but, in the deeper part, low resistivity zones and high resistivity zones are clearly distinguishable. At 256 Hz, a zone that shows slightly-low resistivity values (below 100 Ω -m) is distributed along a NNW line in the eastern part of the area. Expansion and contraction is repeated at several places, and low resistivity spots (below 20 Ω -m) are found near survey points D-30-9, D-34-9, D-37-6 and D-41-6. They also tend to occur in deeper parts. High resistivity zones are found in the western and eastern parts of the area and, in the south, from line D-29 southward, higher resistivity occurs more generally.

Low resistivity zones (below 20 Ω -m) are scattered mostly in the NNW near survey points D-30-9, D-38-6 to D-33-6, D-39-12 and D-41-6 from shallow to deeper parts of the resistivity structure plans.

Resistivity structure, sectional views show a low resistivity value of 5.5 Ω m between 100 and 270 m depths at survey point D-30-12. Notable low resistivity values of 0.2 to 40 Ω -m at points D-37-6 to D-37-15 to depths of 400 m were also found.

Western and southern parts generally show high resistivity. A low resistivity zone, around point D-30-9, is in the geochemical anomaly area, found in the first year survey, where serpentine is distributed.

These results suggest the existence of mineralized zones in serpentinite rocks from shallow to deep parts. Serpentinite, pegmatite, mafic lava and pyroclastic rock, felsitic pyroclastic rock and felsitic sandstone are distributed in the low resistivity zones near survey points D-38-6 to D-33-6, which shows good agreement with the geochemical anomaly around point C-38-6. Mineralized zones in serpentinite in deeper parts are suggested by these results.

Serpentinite is distributed in the low resistivity zones near points D-39-12 and D-41-6, which compares with the weak anomaly in the geochemical exploration.

Area D 2 (Figs. II-13 to 15, Figs. II-16 to 17, Fig. II-24 to 25, Figs. II-28 to 29)

Shallow parts of the apparent resistivity plans and sectional views show complicated resistivity distributions, but low resistivity zones and high resistivity zones are clearly distinguishable in the deeper part. At 16 Hz, a single low resistivity zone, which shows 200 Ω -m or less, is found in the NE direction with an extension range of 200 m, near survey points D-4-6 to D-8-18. The central part has a low resistivity (below 20 Ω -m) running in a NEE direction, with an extension range of about 600 m, from points D-7-12 to D-8-18.

High resistivity zones exist in the western, southern and northern parts of the area, and the deep part shows notably high resistivity values except in the above-mentioned low resistivity zone.

A low resistivity zone in the resistivity structure plans, exists around point D-3-12 and extends deeply. An anomalous zone, around the survey point D-7-15 occurs in the deeper part and shows an eastwards extending tendency. Western and northern parts generally show high resistivity.

Survey point D-7-12, in the resistivity structure sectional views, shows a low resistivity value of 10 Ω -m below 50 m. The deep part at survey point D-4-6 to 9, shows low resistivity values of 10 to 35 Ω -m.

The low resistivity zone around D-3-12 suggests banded ironstone, chert, felsitic sandstone, etc., but no geochemical anomaly was noticed.

Low resistivity around survey point D-7-15, is believed to be caused by the effect of clay-rich layers, etc. in the shallow alluvial layer, but deeper down, mineralized zones are expected in the serpentine rocks on the western side.

Area D 3 (Figs. II-13 to 15, Figs. II-16 to 17, Figs. II-28 to 29)

Relatively low resistance values ($100 \Omega\text{-m}$ or less) are noticed from the apparent resistivity plans and sectional views, from the center to the southern part of the area at shallow depths. Low resistivity zones (below $20 \Omega\text{-m}$) at survey points D-3-33, D-3-45, and D-6-42 in the southern part of the area, are scattered around a high resistivity zone (above $500 \Omega\text{-m}$) near survey point D-4-39. Low resistivity zones (below $20 \Omega\text{-m}$) are noticed near survey points D-9-45, D-7-36 to 42 and D-3-33 in the deeper eastern part of the area. They show notable low resistivity values (below $10 \Omega\text{-m}$) in the central parts.

High resistivity zones are distributed near the above-mentioned point D-4-39 and in the northern part.

Low resistivity zones near point D-3-33 and around points D-7-36 to 7-12 are noticed, from the resistivity structure plans, in the shallow parts. In the deeper part, low resistivity zones occur extensively in the neighborhood of point D-10-48. A low resistivity zone is also noticed near point D-4-45 at the southeastern end of the area. Northern and north-western parts generally show high resistivity.

The area from survey point D-7-33 to D-7-42, in the resistivity structure sectional views, shows low resistivity values (below $10 \Omega\text{-m}$) to depth of 200 m. Point D-4-42 shows a resistivity value as low as $0.3 \Omega\text{m}$ near a depth of 200 m. The low resistivity zone near point D-9-45 has been explored in the past. It almost agrees with the Tynan nickel mineralization zone in serpentine which intruded into sedimentary rocks, banded ironstones, komatiitic basalt and komatiitic pyroclastic rocks. A geochemical anomaly is also noticed. The low resistivity zone near points D-7-36 to 7-42 is associated with the distribution of banded ironstone. It is connected with the previous low resistivity zone, and the existence of deep mineralized zones is expected. A low resistivity zone, near point D-3-33 is associated